Optoelectronic Materials ISSN 2377-4738 *Optoelectron Mater.* ***1*** *(2016) 43–49*

Density functional calculations on the electronic structures of triclinic $ZnMoO_4$

Bao-gai Zhai, Long Yang, Jun-shen Li, Yuan Ming Huang*

School of Mathematics and Physics, Changzhou University, Jiangsu 213164, China

(*Received 12 August 2016; accepted 28 October 2016*)

First principles density functional calculation were carried out to study the electronic structures of triclinic $ZnMoO_4$ crystal. By employing local density approximation (LDA) to describe the exchange–correlation energy, both the band structures and the density of states of perfect and imperfect triclinic $ZnMoO_4$ were calculated. The indirect band gap of perfect triclinic $ZnMoO_4$ is calculated to be 3.46 eV, the top of the valence band of perfect $ZnMoO_4$ has mainly the O 2p character whereas the bottom of the conduction band consists mostly of the Mo 4d states. The defect energy levels of O, Zn and Mo vacancies in the bandgap of $ZnMoO_4$ were determined through the density functional calculations in the framework of LDA scheme. The indirect band gap of $ZnMoO_{(4-\delta)}$ (δ = 0.04) was calculated to be 3.50 eV, and it was found that the oxygen vacancy creates two electron donor levels in the bandgap of $ZnMoO_4$, one of which is located at E_C–0.31 eV while the other is located at E_C–1.00 eV. The indirect band gap of $Zn_{(1-\delta)}MoO_4$ (δ = 0.04) was calculated to be 3.42 eV, the electron acceptor levels created by the Zn vacancy are found to be very close to the top of valence band. As for $ZnMo_{(1-\delta)}O_4$ (δ = 0.04) which bears 4 at.% Mo vacancy, its indirect band gap was calculated to be 3.49 eV, and a series of electron acceptor levels or defect bands were created in the bandgap of the crystal ranging from E_V+0.10 eV to E_V+0.78 eV. The electronic structures derived from the first-principles density functional calculations can be used with reasonable reliability to interpret the orange photoluminescence band of triclinic $ZnMoO_4$, and the oxygen vacancy introduced deep electron donors and are the Mo vacancy introduced deep electron acceptors are considered to be responsible for the orange light emissions from $ZnMoO_4$.

Keywords: Zinc molybdate tetraoxide; Density function theory; Band structure; Bandgap; Defect energy level

1. Introduction

Owing to its excellent optical and electrical performances, zinc molybdate tetraoxide ($ZnMoO_4$) is an important inorganic material with wide applications in catalysis [1], humidity sensors [2], battery materials [3], photoluminescence [4,5], anticorrosive paints [6], and croyogenic photon-scintillation detectors [7-11]. It is known that $ZnMoO_4$ can be found in nature with two different types of crystalline phase: the triclinic phase and the monoclinic phase. In the triclinic $ZnMoO_4$ structure, the Mo atoms are coordinated to four oxygen atoms, resulting in the tetrahedral [MoO_4] clusters [12], but Zn atoms exhibit three kinds of configurations by bonding to five and six oxygen atoms to form distorted pentahedral, hexahedral and octahedral clusters, respectively. The triclinic $ZnMoO_4$ belongs to the wolframite-type metal molybdates. On the other hand, the monoclinic $ZnMoO_4$ structure has both Zn and Mo atoms bonded to six oxygen atoms, which promote the origin of distorted octahedral [ZnO_6] and [MoO_6] clusters, respectively [13].

Triclinic $ZnMoO_4$ is in itself an efficient luminescent material. For example, undoped $ZnMoO_4$ exhibits a broad photoluminescence (PL) band with its maximum at around 2 eV (620 nm) [14-17]. As estimated from the transmittance and absorption spectra in the literature, the bandgap of $ZnMoO_4$ is around 4.0 eV [9,10,14,16,17]. Thus the band edge recombination cannot be responsible for the recorded orange PL band. In other words, the orange PL band with its maximum at around 2 eV should be originate from the defect emission in triclinic $ZnMoO_4$. In order to understand its luminescent properties, it is critically important to determine the defect energy levels in the bandgap of triclinic $ZnMoO_4$. It is well known that both the electrical and the optical properties of semiconductors can be modified significantly by the presence of point defects and impurities. Most notably, the electrical conductivity of semiconductors is drastically enhanced by the incorporation of small amounts of impurities, which is the foundation underlying modern electronic devices. Hence, the understanding of the role of defects and the ability to control them are thus of great importance in the development of semiconductor devices. However, the determination of the defect energy levels in the bandgap of triclinic $ZnMoO_4$ is still not investigated experimentally or theoretically, although Spassky et al. performed ab initio calculations using the full-potential linear-augmented-plane-wave method method with the local density approximation (LDA) implemented in the WIEN 2k code for the triclinic phase of perfect $ZnMoO_4$ crystal [18]. It is obvious that the undetermined defect energy levels of defect-bearing $ZnMoO_4$ hamper the understanding on the luminescent properties of triclinic $ZnMoO_4$.

First-principles calculations have long been recognized as an indispensable tool in the characterization of defects [19,20]. As documented in the literature, density functional theory (DFT) calculations can provide important information on the electronic and optical properties of diverse materials without employing any empirical parameters, and a number of density functional calculations were explored to compute the electronic structures of luminescent materials in the framework of the LDA scheme, the generalized gradient approximation (GGA) scheme, or the meta generalized gradient approximation (meta GGA) scheme [21-26]. The increasing accuracy resulting from the fast development of theoretical methods also enables a reliable prediction of defect properties which would otherwise remain inaccessible in experiments. In this work, we calculated the band structures and density of states (DOS) of both

*Corresponding author. Email: dongshanisland@126.com

perfect and imperfect $ZnMoO_4$ by employing LDA scheme to describe the exchange correlation functional in the framework of DFT. The band structures and density of states of both perfect and imperfect $ZnMoO_4$ were gained by using the first-principles DFT calculations. The defect energy levels of O, Zn and Mo vacancies in $ZnMoO_4$ were determined through DFT calculations in the framework of LDA scheme. The derived defect energy levels of O, Zn and Mo vacancies through the first principles DFT calculations can considerably shed fresh insight on the orange PL band of triclinic $ZnMoO_4$.

Table 1 Fractional coordinates of atoms in the unit cell of triclinic $ZnMoO_4$. Unit cell parameters of $ZnMoO_4$ are a = 0.9625 nm, b = 0.6965 nm, c = 0.8373 nm, α = 103.28º, β = 96.30º, γ = 106.72º.

Atom No	Atoms	*x*	*y*	*z*
1	Mo	0.3409	0.1999	0.1036
2	Mo	0.6591	0.8001	0.8964
3	Mo	0.1251	0.5208	0.7967
4	Mo	0.8749	0.4792	0.2043
5	Mo	0.2559	0.0048	0.4885
6	Mo	0.7441	0.9952	0.5115
7	O	0.1447	0.9504	0.6300
8	O	0.8553	0.0496	0.3700
9	O	0.2635	0.7637	0.3670
10	O	0.7365	0.2363	0.6330
11	O	0.1830	0.1494	0.3605
12	O	0.8170	0.8506	0.6395
13	O	0.1509	0.0580	0.0210
14	O	0.8491	0.9420	0.9790
15	O	0.2172	0.5212	0.6272
16	O	0.7828	0.4788	0.3728
17	O	0.6416	0.5493	0.7668
18	O	0.3584	0.4507	0.2332
19	O	0.2513	0.6484	0.9838
20	O	0.7487	0.3516	0.0162
21	O	0.5712	0.8414	0.4060
22	O	0.4288	0.1586	0.5940
23	O	0.0393	0.2664	0.8009
24	O	0.9607	0.7336	0.1991
25	O	0.0143	0.3559	0.2315
26	O	0.9857	0.6441	0.7685
27	O	0.5738	0.7532	0.0624
28	O	0.4262	0.2468	0.9376
29	O	0.4268	0.0596	0.2100
30	O	0.5732	0.9404	0.7900
31	Zn	0.4094	0.7508	0.1946
32	Zn	0.5906	0.2492	0.8054
33	Zn	0.9886	0.0353	0.1943
34	Zn	0.0114	0.9647	0.8057
35	Zn	0.2138	0.4677	0.3870
36	Zn	0.7862	0.5323	0.6130

2. Computational methodology

First-principles DFT calculations of the band structures of $ZnMoO_4$ with various defects were performed using the DFT module of the Quantumwise Atomistix ToolKit 11.8 package. The exchange–correlation functional was treated within the LDA scheme, in which the exchange potential was parameterized by Perdew and Zunger [27]. Triclinic $ZnMoO_4$ belongs to space group $P\bar{1}$. There were 6 Zn, 6 Mo and 24 O atoms in the unit cell of $ZnMoO_4$. The parameters of triclinic $ZnMoO_4$ were a = 0.9625 nm, b = 0.6965 nm, c = 0.8373 nm, α = 103.28, β = 96.30 and γ = 106.72º. The considered electronic configurations were $3d^{10}4s^24p^0$ for Zn, $2s^22p^4$ for O, $4p^64d^55s^1$ for Mo. Double zeta single polarized basis sets were chosen for each element. The electronic wavefunctions were expanded in plane waves up to a kinetic energy cut-off with a typical value of 100 Hartree. The Brillouin zone was sampled by a 5 × 5 × 5 Monkhorst-Pack mesh of k points. The Brillouin zone sampling and the kinetic energy cutoff were sufficient to guarantee an excellent convergence for the calculated band structures. The tolerance of the calculation was 4×10^{-5} eV.

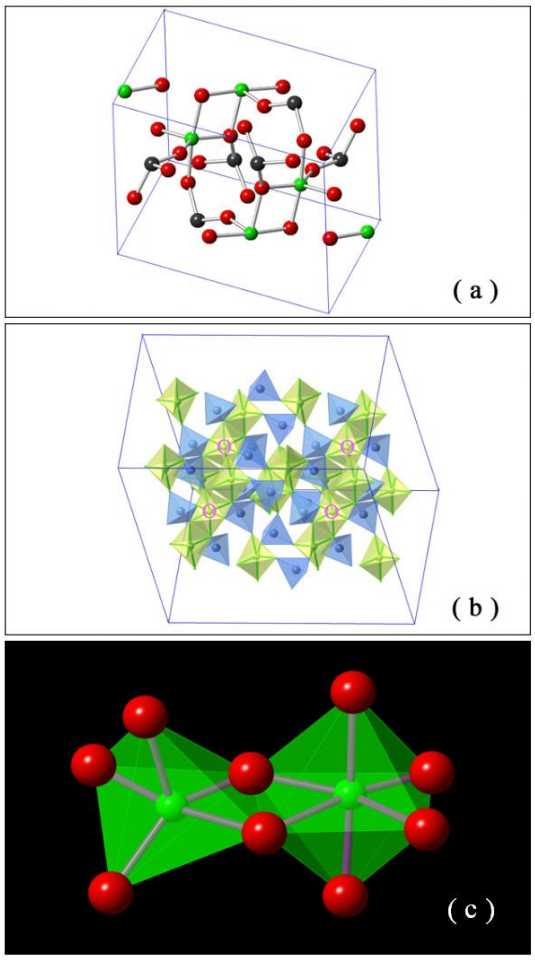

Fig. 1 (a) Unit cell of triclinic $ZnMoO_4$. The black, red and green balls represent Mo, O and Zn atoms, respectively. (b) The schematic view of the triclinic $ZnMoO_4$ to show the Zn-O hexahedrons and octahedrons as marked by the capital letter O. (c) Individual Zn-O hexahedron and octahedron in $ZnMoO_4$.

3. Results and discussion

3.1 Crystal structure of perfect triclinic $ZnMoO_4$

It is well known that $ZnMoO_4$ has two crystalline phases, i.e., the triclinic $ZnMoO_4$ and the monoclinic $ZnMoO_4$. Triclinic $ZnMoO_4$ is a thermodynamically

stable compound than the monoclinic phase. Fig. 1(a) shows the unit cell of triclinic $ZnMoO_4$. As shown in Fig. 1(a), the triclinic $ZnMoO_4$ has a crystal structure with six formula units per unit cell. There are 6 Zn, 6 Mo and 24 O atoms in the unit cell of the triclinic phase of $ZnMoO_4$. The unit cell parameters are a = 0.9625 nm, b = 0.6965 nm, c = 0.8373 nm, $\alpha = 103.28^o$, $\beta = 96.30^o$, $\gamma = 106.72^o$, respectively. The space group of the triclinic $ZnMoO_4$ is $P\bar{1}$ (no. 2). The fractional coordinates of the atoms in the unit cell of $ZnMoO_4$ are listed in Table 1. Fig. 1(b) represents the schematic view of the triclinic $ZnMoO_4$. It can be seen that triclinic $ZnMoO_4$ is characteristic of MoO_4 tetrahedra and ZnO polyhedra. The ZnO hexahedra and ZnO octahedra in Fig. 1(b) are marked with the capital letter ***O*** for the purpose of clarity. In addition to the ZnO hexahedra and ZnO octahedra in Fig. 1(b), ZnO pentahedra can be identified at the corners of Fig. 1(b). Fig. 1 (c) shows individual ZnO hexahedron and octahedron in $ZnMoO_4$. It is clear that the Zn^{2+} ions in ZnO hexahedron and octahedron are coordinated to 5 and 6 oxygen atoms, respectively.

3.2 Electronic structures of perfect $ZnMoO_4$

Fig. 2 illustrates the calculated band structures of perfect triclinic $ZnMoO_4$ using DFT within the framework of LDA scheme. Double zeta single polarized LCAO basis set was chosen for each element in $ZnMoO_4$. The origin of the energy scale is chosen at the top of the valence band (VB). As follows from the DFT calculations, the conduction band (CB) minimum (3.46 eV) is reached at the X point, the VB maximum (0 eV) can be found in the R point. Therefore, triclinic $ZnMoO_4$ crystal can be considered as an indirect gap material whose calculated band gap value equals 3.46 eV. According to the report given by Spassy et al., the uncorrected indirect bandgap of triclinic $ZnMoO_4$ equals 3.62 eV when using the full-potential linear-augmented-plane-wave method with the LDA implemented in the WIEN 2k code for the triclinic phase of perfect $ZnMoO_4$ crystal [18]. A comparison with previously reported data for triclinic $ZnMoO_4$ using the full potential linear augmented plane wave method reveals that our calculated value is only 0.16 eV lower than the band gap value derived by Spassky et al [18]. It should be noted that the band gap value obtained directly from our calculations should be somewhat corrected using experimental data. As estimated from the transmittance and absorption spectra in the literature, the bandgap of triclinic $ZnMoO_4$ should be no less than 4.0 eV [3,4,6,8,9]. It is known that the band gap of a crystal may be underestimated if calculations are made under the DFT formalism. Mainstream theoretical studies rest on Kohn–Sham (KS) DFT, a framework that is now widely adopted in electronic structure calculations. The many-body effect in DFT is described by the exchange-correlation (xc) functional, but its exact form is unavailable and approximations have to be made. Typical (semi)local approximations include the LDA and the GGA. With LDA and GGA functionals, the calculated KS band gaps of materials are subject to severe underestimations amounting up to 50% of experimental band gaps. This is often referred to as the 'band-gap problem' and its origin has been tracked down to the spurious self-interaction and the lack of derivative discontinuity in the approximate xc functionals. Thus the band gap of a crystal may be underestimated if calculations are made under the DFT formalism. To overcome this drawback, the correcting energy addition to E_g or the 'scissor operator' is introduced at the stage of calculation of the optical parameters. Then the value of Δ is obtained from the best fit between the calculated optical spectra and the corresponding experimental data. If we apply this procedure to the triclinic $ZnMoO_4$ crystal, the CB should be upshifted 0.54 eV so that the band gap equals 4.0 eV, suggesting the scissor operator value Δ = 0.54 eV.

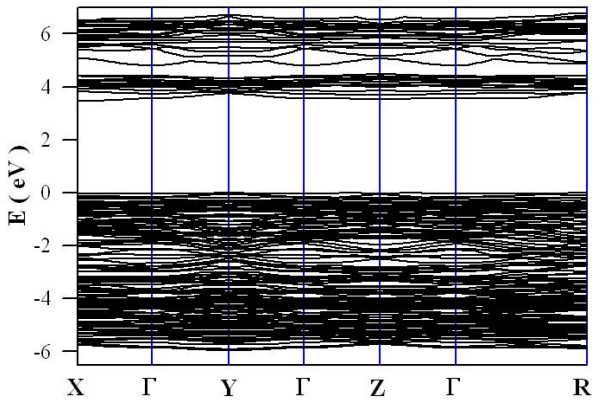

Fig. 2 Calculated band structures of perfect triclinic $ZnMoO_4$ using DFT within the framework of LDA scheme. Double zeta single polarized LCAO basis set was chosen for each element in $ZnMoO_4$.

The calculated total DOS and projected DOS of triclinic $ZnMoO_4$ are presented in Fig. 3. The origin of the energy scale is chosen at the top of the valence band. As can be seen in Fig. 3, the Zn 3d, Mo 4d and O 2p contribute significantly to the VB of the crystal in the range of -6 to 0 eV. As a contrast, the contributions of the other types of electronic states to the VB is insignificant in the range of -6 to 0 eV. Examples of such include the electronic states O 2s, Zn 4s Zn 4p, Mo 4p and Mo 5s. Actually, the O 2s state contributes to the core band of the crystal, which is located 10 eV below the bottom of the VB. The Mo 4p states also have some contributions to this core band. Further analysis of Fig. 3 shows that the top of the VB is formed by O 2p and Zn 3d states whereas Mo 4d state has no significant contribution. The contribution of Zn 3d states becomes dominant in the lower part of the VB with their peaks notable in the range of -4 to -6 eV. As shown recently by electronic structure calculations for $CdMoO_4$, $CaMoO_4$, $PbWO_4$, $CaWO_4$ and $PbMoO_4$, such absence of W (Mo) states at the top of the VB is characteristic of tungstate and molybdate crystals. This feature is typical for the electronic structure of transition metal complexes XO_4^{2-} (X = Cr, Mo, W). Almost all methods of electronic structure calculations show that the highest occupied molecular orbital of such a complex is formed purely by O 2p states.

Similar analysis is applied to CB of the triclinic $ZnMoO_4$. According to the DFT calculations, the Mo 4d

states (with some contribution from O 2p states) clearly dominate in the CB below 4.8 eV. The O 2s, Zn 3d, Mo 4p and Mo 5s states are practically absent in the bottom of CB. However, some contributions of Zn 4s and Zn 4p can be identified in the bottom of the CB. Therefore, Fig. 3 has demonstrated that the top of the VB of $ZnMoO_4$ has mainly the O 2p character whereas the bottom of the CB consists mostly of the Mo 4d states.

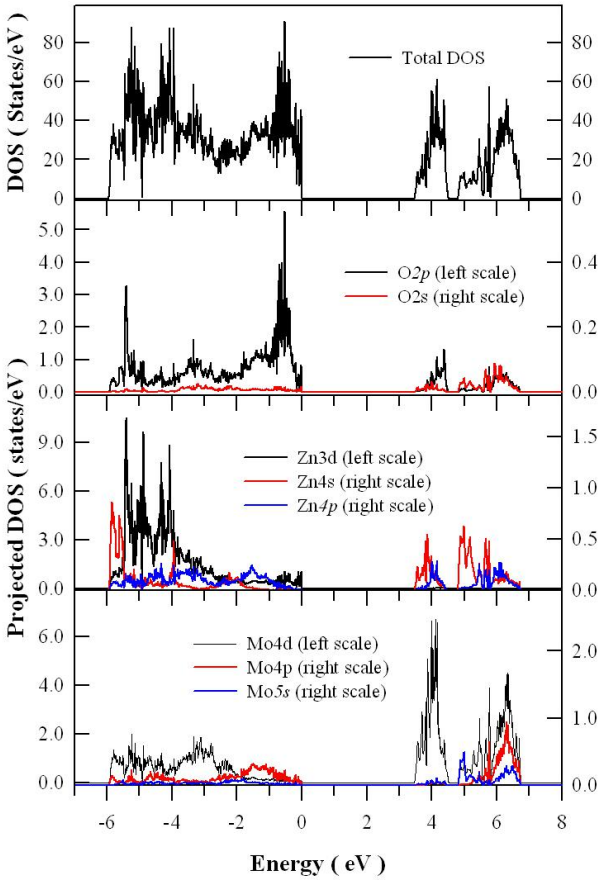

Fig. 3 Calculated total DOS and projected DOS of perfect triclinic $ZnMoO_4$ using DFT in the framework of LDA scheme. Double zeta single polarized LCAO basis set was chosen for each element in $ZnMoO_4$.

3.3 Electronic structures of imperfect $ZnMoO_4$ bearing O, Zn and Mo vacancies

Fig. 4 shows the DFT calculated band structures and total DOS of oxygen vacancy containing $ZnMoO_4$. Double zeta single polarized LCAO basis set was chosen for each element in $ZnMoO_4$. A 2×2×1 super cell is constructed to contain 24 Zn sites, 24 Mo sites and 96 O sites. One oxygen site is taken away from the lattice with the result of $ZnMoO_{(4-\delta)}$ where $\delta = 0.04$. In $ZnMoO_{(4-\delta)}$ ($\delta = 0.04$), about 1 at% O sites in the lattice are vacant. As shown in Fig. 4, the VB maximum (0 eV) is located at X point whereas the CB minimum is located at Gamma point. Consequently, the O vacancy containing $ZnMoO_4$ keeps its nature as an indirect semiconductor. The indirect band gap is measured to be 3.50 eV. When compared to the bandgap value of perfect $ZnMoO_4$ (3.46 eV), the imperfect $ZnMoO_4$ bearing about 1 at% O vacancies exhibits a little bit wider band gap (0.06 eV). The band gap is a property of the lattice constant, and the band gap can be changed by varying the lattice constant. The lattice constant can be changed by various ways, e.g by applying pressure by heating or cooling or by mixing with another semiconductor. Both the direct and the indirect band gap will change with the lattice constant but at different rates. Hence the recorded increase in the bandgap value can be attributed to the changes in the lattice constant of triclinic $ZnMoO_4$. The other most prominent feature in Fig. 4 is that two electron donor levels are created in the bandgap of $ZnMoO_4$ by the O vacancy. One of the electron donor levels is located at E_C–1.00 eV whereas the other is located at E_C–0.31 eV. The two deep electron donors may play important roles in the recorded orange light emissions from triclinic $ZnMoO_4$.

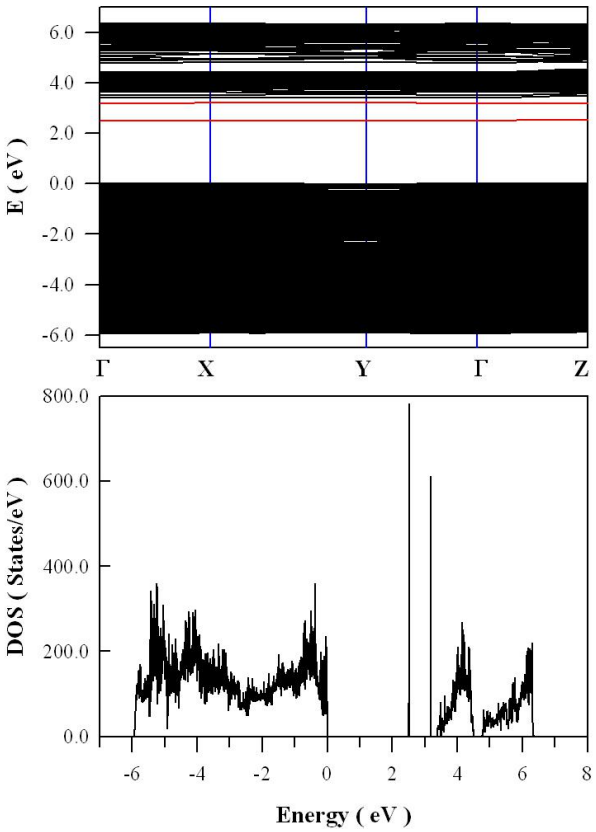

Fig. 4 Calculated band structures and total DOS of oxygen vacancy containing $ZnMoO_4$ using DFT within the framework of LDA scheme. Double zeta single polarized LCAO basis set was chosen for each element in $ZnMoO_4$.

Fig. 5 shows the calculated band structures and total DOS of imperfect $ZnMoO_4$ bearing Zn vacancy. Double zeta single polarized LCAO basis set was chosen for each element in $ZnMoO_4$. A 2×2×1 super cell is constructed to contain 24 Zn sites, 24 Mo sites and 96 O sites. One Zn site is taken away from the lattice with the result of $Zn_{(1-\delta)}MoO_4$ where $\delta = 0.04$. In $Zn_{(1-\delta)}MoO_4$ ($\delta = 0.04$), about 4 at.% Zn sites in the lattice are vacant. As shown in Fig. 5, the VB maximum and the CB minimum are located at different k points, indicating that the Zn vacancy containing $ZnMoO_4$ keeps its nature as an indirect semiconductor. The indirect band gap is calculated to be 3.42 eV. When compared to the bandgap value of perfect $ZnMoO_4$ (3.46 eV), the imperfect

$ZnMoO_4$ bearing about 4 at% Zn vacancies exhibits a little bit narrower band gap (0.04 eV). The second most prominent feature in Fig. 5 is that some electron acceptor levels are created in the bandgap of $ZnMoO_4$ by the Zn vacancy. Unlike the deep electron donor levels in Fig. 4, the Zn vacancy introduced electron acceptor levels are shallow, they are very close to the top of VB. These shallow electron acceptor levels are located within 100 meV above the VB maximum, so they are not likely to be responsible for the recorded orange PL band of triclinic $ZnMoO_4$.

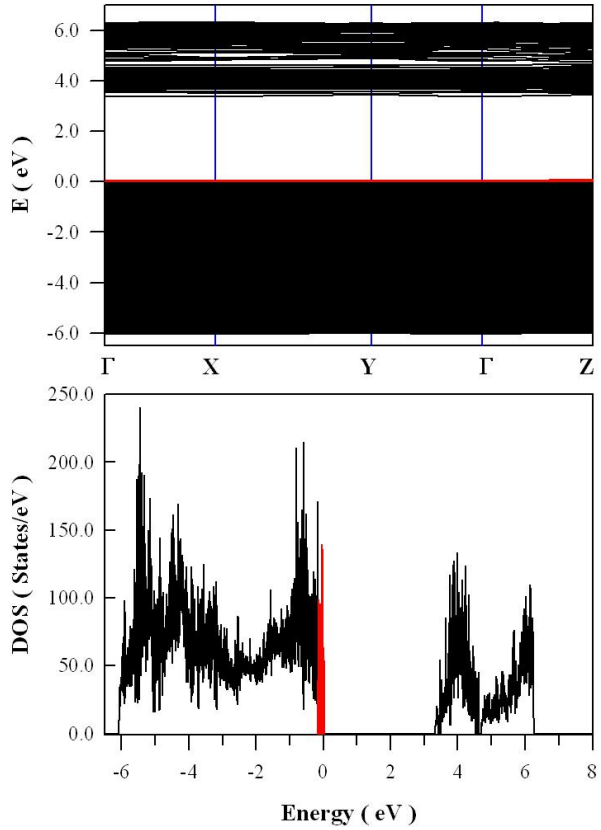

Fig. 5 Calculated band structures and total DOS of zinc vacancy containing $ZnMoO_4$ using DFT within the framework of LDA scheme. Double zeta single polarized LCAO basis set was chosen for each element in $ZnMoO_4$.

Fig. 6 shows the calculated band structures and total DOS of Mo vacancy containing $ZnMoO_4$ by using DFT within the framework of LDA scheme. Double zeta single polarized LCAO basis set was chosen for each element in $ZnMoO_4$. A 2×2×1 super cell is constructed to contain 24 Zn sites, 24 Mo sites and 96 O sites. One Mo site is taken away from the lattice with the result of $ZnMo_{(1-\delta)}O_4$ where $\delta = 0.04$. In $ZnMo_{(1-\delta)}O_4$ ($\delta = 0.04$), about 4 at.% of Mo sites in the lattice are vacant. As shown in Fig. 6, the VB maximum and the CB minimum are located at different k points, indicating that the Mo vacancy containing $ZnMoO_4$ still keeps its nature as an indirect semiconductor. The indirect band gap is calculated to be 3.49 eV. When compared to the bandgap value of perfect $ZnMoO_4$ (3.46 eV), the imperfect $ZnMoO_4$ bearing about 4 at% Mo vacancies exhibits a little bit wider band gap (0.03 eV). It is noted that a series of electron acceptor levels are created in the bandgap of $ZnMoO_4$. They are distributed in the range of E_V+0.10 eV to E_V+0.78 eV.

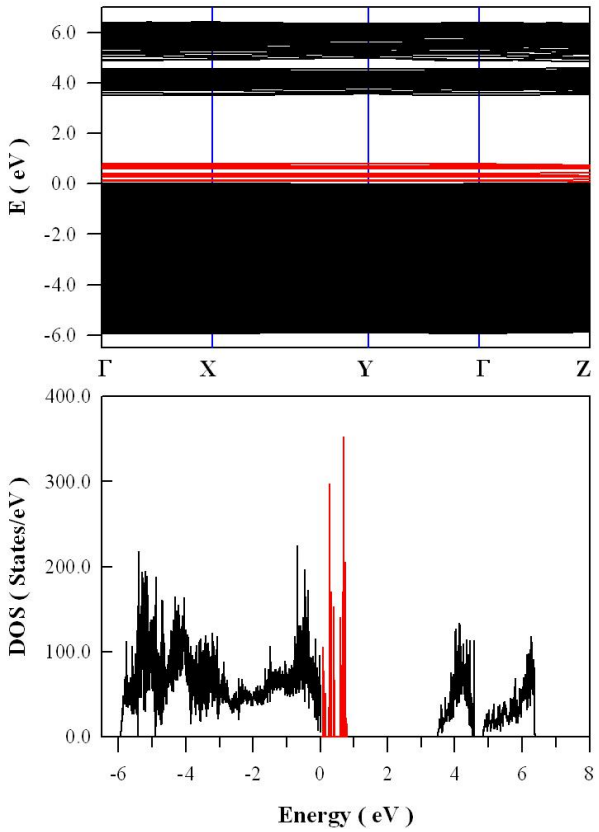

Fig. 6 Calculated band structures and total DOS of Mo vacancy containing $ZnMoO_4$ using DFT within the framework of LDA scheme. Double zeta single polarized LCAO basis set was chosen for each element in $ZnMoO_4$.

3.4 Band diagram of triclinic $ZnMoO_4$ bearing O, Zn and Mo vacancies

The bandgap problem in DFT is well-known. A common way to alleviate this problem is to apply a 'scissor' operation whereby the CBs are shifted in energy by a constant amount so that the band gap matches known experimental observations. It is obvious that the calculated bandgap in Figs. 4-6 are underestimated. On the basis of our reflectance spectral characterization on $ZnMoO_4$, the bandgap of triclinic $ZnMoO_4$ is around 4.10 eV [9,10,14,16,17]. In order to keep the bandgap value of 4.10 eV for $ZnMoO_4$, the scissor operation can be applied to the calculated band structures in Fig. 4 by shifting each CB upwards 0.64 eV to match the bandgap value 4.10 eV for perfect $ZnMoO_4$. Fig. 7 shows the band diagram of triclinic $ZnMoO_4$ bearing O, Zn and Mo vacancies. The intrinsic point defects in $ZnMoO_4$ are represented by V_O, V_{Al} and V_{Mo}. Before the bandgap correction, V_O introduces two electron donor levels at E_C–0.31 and E_C–1.00 eV in the bandgap of triclinic $ZnMoO_4$, as demonstrated in Fig. 4. In stead of rigidly shifting up the defect levels, a more practical approach to correct the band gap is to use the so-called scissors operator whereby the entire conduction band is shifted up in energy so that it matches with the experimentally observed band gap. By applying the scissor operator, all the calculated defect

levels are scaled by a fraction k, the ratio of the experimental to the calculated band gap. In order to keep the band gap of $ZnMoO_4$ to be 4.10 eV, we applied the scissors operation to Fig. 4 by shifting the CB upwards 0.64 eV. After using the scissors operator ratio k = 4.10/3.46 = 1.185 for the correction, the band gap of $ZnMoO_4$ with V_O is 4.10 eV, the V_O introduced two electron donor levels are located at E_C–0.37 eV and E_C–1.19 eV, respectively. As for Zn vacancies in $ZnMoO_4$, they create shallow electron acceptor levels within 100 meV above the VB maximum, so they are still very close to the VB after the scissors operation. For the clarity of the band diagram, we do not show them in Fig. 7. But the case changes for Mo vacancies $ZnMoO_4$. Before scissors operation, Mo vacancies create a narrow defect band in the bandgap of $ZnMoO_4$, which are distributed in the range of E_V+0.10 eV to E_V+0.78 eV, as shown in Fig. 6. After using the scissors operator ratio k = 1.185 for the correction, the defect band gap of $ZnMoO_4$ with V_{Mo} ranges from E_V+0.12 eV to E_V+0.92 eV. The corrected defect band is depicted in Fig. 7 with a narrow band for Mo vacancies.

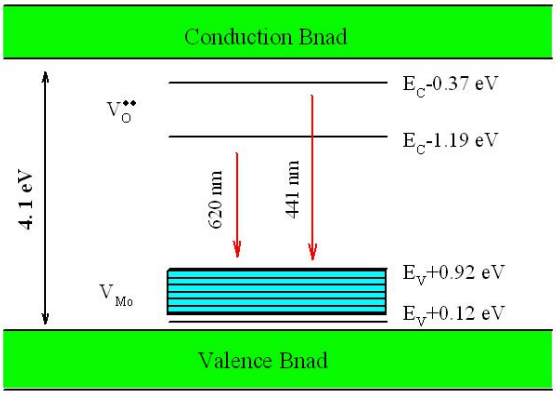

Fig. 7 Schematic illustrations on the defect energy levels and visible photoluminescence of triclinic $ZnMoO_4$ crystals.

On the basis of Fig. 7, the energy difference between the electron donor level E_C–1.19 eV of V_O and the electron acceptor level E_V+0.92 eV of V_{Mo} is 1.99 eV, so the recombination from E_C-1.19 eV to E_V+0.92 eV will result in visible light emission with its wavelength at 620 nm. In a similar way, the energy difference between the electron donor level E_C-0.37 eV of V_O and the electron acceptor level E_V+0.92 eV of V_{Mo} is 2.81 eV, so the recombination from E_C-0.37 eV to E_V+0.92 eV will result in visible light emission with its wavelength at 441 nm. The prediction in Fig. 7 is justified by the broad PL band centered at around 2 eV (620 nm) for triclinic $ZnMoO_4$ [14-17]. Thus, the O and Mo vacancies are proposed to play important roles in the recorded orange light emissions from triclinic $ZnMoO_4$.

4. Conclusion

By employing LDA to describe the exchange–correlation energy, the band structures and DOS of perfect and imperfect triclinic $ZnMoO_4$ were calculated with density functional theory. The defect energy levels of O, Zn and Mo vacancies in the bandgap of $ZnMoO_4$ were determined through DFT calculations in the framework of LDA scheme. The calculated bandstructures and DOS are presented to aim at the understanding of the visible emission band from $ZnMoO_4$. The indirect band gap of perfect triclinic $ZnMoO_4$ is calculated to be 3.46 eV, the top of the VB of perfect $ZnMoO_4$ has mainly the O 2p character, whereas the bottom of the CB consists mostly of the Mo 4d states. The defect energy levels of O, Zn and Mo vacancies in the bandgap of $ZnMoO_4$ were determined through DFT calculations in the framework of LDA scheme. For $ZnMoO_{(4-\delta)}$ (δ = 0.04) which bears 1 at.% O vacancy, its indirect band gap is calculated to be 3.50 eV, and two electron donor levels are created by the oxygen vacancy, one is located at E_C-1.00 eV, the other is located at E_C-0.31 eV. The two deep electron donors may play important roles in the visible light emissions from $ZnMoO_4$. For $Zn_{(1-\delta)}MoO_4$ (δ = 0.04) in which 4 at.% Zn sites are vacant, its indirect band gap is 3.42 eV, and three electron acceptor levels are created close to the top of valence band. For $ZnMo_{(1-\delta)}O_4$ (δ = 0.04) in which 4 at.% of Mo sites are vacant, its indirect band gap is 3.49 eV. A series of electron acceptor levels are created above the top of valence band in the range of E_V+0.10 eV to E_V+0.78 eV. The electronic structures derived from the first-principles density functional calculations can be used with reasonable reliability to interpret the defect emission of triclinic $ZnMoO_4$. The results are discussed in view of interpreting the broad emission band at about 2 eV of triclinic $ZnMoO_4$.

Acknowledgment

The authors would like to acknowledge the financial support from National Natural Science Foundation of China under the grant numbers 11574036 and 1604028.

References

[1] H. Fu, J. Lin, L. Zhang, Y. Zhu, Photocatalytic activities of a novel $ZnWO_4$ catalyst prepared by a hydrothermal process, *Appl. Catal. A* 306 (2006) 58 – 67.

[2] A.M. Edwin Suresh Raj C. Mallika, K. Swaminathan, O.M. Sreedharan, K.S. Nagaraja, Zinc(II) oxide–zinc(II) molybdate composite humidity sensor, *Sens. Actuat. B – Chem.* 81 (2002) 229 – 36.

[3] N.N. Leyzerovich, K.G. Bramnik, T. Buhrmester, H. Ehrenberg, H. Fuess, Electrochemical intercalation of lithium in ternary metal molybdates $MMoO_4$ (M: Cu, Zn, Ni and Fe), *J. Power Sources* 127 (2004) 76 – 84.

[4] L.S. Cavalcante, J.C. Sczancoski, M. Siu Li, E. Longo, J.A. Varela, β -$ZnMoO_4$ microcrystals synthesized by the surfactant-assisted hydrothermal method: Growth process and photoluminescence properties. *Colloid Surface A* 396 (2012) 346–351.

[5] D. Spassky, A. Vasilev, I. Kamenskikh, V. Kolobanov, V. Mikhailin, A. Savon, L. Ivleva, I. Voronina, L. Berezovskaya, Luminescence investigation of zinc molybdate single crystals, *Phys. Stat. Sol. A* 206 (2009) 1579–1583.

[6] B.D. Amo, R. Romagnoli, V.F. Vetere, Performance of zinc molybdenum phosphate in anticorrosive paints by accelerated and electrochemical tests, *J. Appl. Electrochem.* 29 (1999) 1401–1407.

[7] L. Gironi, Scintillating bolometers for Double Beta Decay search, *Nucl. Instrum. Method A* 617 (2010) 478–481.

[8] L. Gironi, C. Arnaboldi, J.W. Beeman, O. Cremonesi, F.A.

Danevich, V.Ya. Degoda, L.I. Ivleva, L.L. Nagornaya, M. Pavan, G. Pessina, S. Pirro, V.I. Tretyak, I.A. Tupitsyna, Performance of $ZnMoO_4$ crystal as cryogenic scintillating bolometer to search for double beta decay of molybdenum, *J. Instr.* (2010) 11007.

[9] L.L. Nagornaya, F.A. Danevich, A.M. Dubovik, B.V. Grinyov, S. Henry, V. Kapustyanyk, H. Kraus, D.V. Poda, V.M. Kudovbenko, V.B. Mikhailik, M. Panasyuk, O.G. Polischuk, V. Rudyk, V. Tsybulskyi, I.A. Tupitsyna, Yu. Ya, Vostretsov, Tungstate and molybdate scintillators to search for dark matter and double beta decay, *IEEE Trans. Nucl. Sci.* 56 (2009) 2513.

[10] D.M. Chernyak, F.A.Danevich, V.Ya.Degoda, I.M.Dmitruk, F.Ferri, E.N.Galashov, A.Giuliani, I.M.Ivanov, V.V.Kobychev, M.Mancuso, S.Marnieros, V.M. Mokina, C.Nones, E.Olivieri, G.Pessina, C.Rusconi, V.N.Shlegel, O.P.Stanovyi, M.Tenconi, V.I.Tretyak, I.A.Tupitsyna, Optical, luminescence and thermal properties of radiopure $ZnMoO_4$ crystals used in scintillating bolometers for double beta decay search, *Nucl. Instrum. Method. A* 729 (2013)856–863.

[11] J.W. Beeman, F. Bellini, P. Benetti, L. Cardani, N. Casali, D. Chiesa, M. Clemenza, I. Dafinei, S. Di Domizio, F. Ferroni, A. Giachero, L. Gironi, A. Giuliani, C. Gotti, M. Maino, S. Nagorny, S. Nisi, C. Nones, F. Orio, L. Pattavina, G. Pessina, G. Piperno, S. Pirro, E. Previtali, C. Rusconi, M. Tenconi, C. Tomei, M. Vignati, Current status and future perspectives of the LUCIFER experiment, *Adv. High Energy Phys.* 2013 (2013) 237973.

[12] W. Reichelt, T. Weber, T. Sohnel, S. Dabritz, Mixed crystals in the system $CuMoO_4/ZnMoO_4$, *Z. Anorg . Allg. Chem.* 626 (2000) 2020–2027.

[13] K. Pavani, A. Ramanan, Influence of 2-aminopyridine on the formation of molybdates under hydrothermal conditions, *Eur J Inorg Chem* 15 (2005) 3080–3087.

[14] Y.R. Jiang, W.W. Lee, KT. Chen, M.C. Wang, K.H. Chang, C.C. Chen, Hydrothermal synthesis of β -$ZnMoO_4$ crystals and their photocatalytic degradation of Victoria Blue R and phenol, *J.Taiwan Inst. Chem. E.* 45 (2014) 207–218

[15] V.B. Mikhailik, H. Kraus, D. Wahl, H. Ehrenberg, M.S. Mykhaylyk, Optical and luminescence studies of $ZnMoO_4$ using vacuum ultraviolet synchrotron radiation, *Nucl. Instrum. Method. A* 562 (2006) 513–516.

[16] D.A. Spassky, V.V. Mikhailin, A.E. Savon, E.N. Galashov, V.N. Shlegel, Ya.V. Vasiliev, Low temperature luminescence of $ZnMoO_4$ single crystals grown by low temperature gradient Czochralski technique, *Opt. Mater.* 34 (2012) 1804–1810.

[17] B.G. Zhai, L. Yang, Q.L. Ma, Y.M. Huang, Growth of $ZnMoO_4$ nanowires via vapor deposition in air, *Mater. Lett.* 188 (2017) 119–122.

[18] D.A. Spassky, I.A. Kamenskikh, A.E. Savon, S.G. Nedilko, P.A. Lykov, Electronic structure and luminescence mechanisms in $ZnMoO_4$ crystals, *J. Phys. Condens. Mat.* 23 (2011) 365501.

[19] W. Chen, A. Pasquarello, First-principles determination of defect energy levels through hybrid density functionals and GW, *J. Phys. – Condens. Mat.* 27 (2015) 133202

[20] H. Gudmundsdóttir, E.Ö. Jónsson, H. Jónsson, Calculations of Al dopant in α -quartz using a variational implementation of the Perdew – Zunger self-interaction correction, *New J. Phys.* 17 (2015) 083006.

[21] B.G. Zhai, L. Yang, Q.L. Ma, Y.M. Huang, Visible light driven photocatalytic activity of Fe-doped ZnO nanocrystals, *Funct. Mater. Lett.* 10 (2017) 1750002.

[22] B.G. Zhai, Q.L. Ma, Y.M. Huang, Instability of the characteristic emissions of dopant Tb in ZnO hexagonal pyramids, *J. Electron. Mater.* 46 (2017) 947–957.

[23] B.G. Zhai, Y.M. Huang, Green photoluminescence and afterglow of Tb doped $SrAl_2O_4$, *J. Mater. Sci.* 52 (2017) 1813–1822.

[24] B.G. Zhai, L. Yang, Q.L. Ma, X. Liu, Y.M. Huang, Mechanism of the prolongation of the green afterglow of $SrAl_2O_4:Dy^{3+}$ caused by the use of H_3BO_3 flux, *J. Lumin*. 181 (2017) 78–87.

[25] B.G. Zhai, L. Yang, Q.L. Ma, Y.M. Huang, First-principles calculations of band structures and optical properties of hexagonal ZnO by using meta-GGA in the framework of density functional theory, *Optoelectron. Mater.* 1 (2015) 13–17.

[26] B.G. Zhai, C. Tang, Y.M. Huang, First-principles density functional calculations of the band structures of $SrAl_2O_4$, *Optoelectron. Mater.* 1 (2015) 18–21.

[27] J.P. Perdew, A, Zunger, Self-interaction correction to density-functional approximations for many-electron systems, *Phys. Rev. B* 23 (1981) 5048–5078.